Aerosol and Air Quality Research, 17: 3166–3178, 2017

ISSN: 1680-8584 print / 2071-1409 online
doi: 10.4209/aaqr.2017.05.0185

A Simulation Study on $PM_{2.5}$ Sources and Meteorological Characteristics at the Northern Tip of Taiwan in the Early Stage of the Asian Haze Period

Ming-Tung Chuang[1*], Charles C.-K. Chou[2], Neng-Huei Lin[3], Akinori Takami[4], Ta-Chih Hsiao[5], Tang-Huang Lin[6], Joshua S. Fu[7], Shantanu Kumar Pani[3], Yun-Ru Lu[1], Tsung-Yeh Yang[1]

[1] *Graduate Institute of Energy Engineering, National Central University, Taoyuan 32001, Taiwan*
[2] *Research Center for Environmental Changes, Academia Sinica, Taipei 11529, Taiwan*
[3] *Department of Atmospheric Sciences, National Central University, Taoyuan 32001, Taiwan*
[4] *Center for Regional Environmental Research, National Institute for Environmental Studies, Ibaraki 305-8506, Japan*
[5] *Graduate Institute of Environmental Engineering, National Central University, Taoyuan 32001, Taiwan*
[6] *Center for Space and Remote Sensing Research, National Central University, Taoyuan 32001, Taiwan*
[7] *Department of Civil and Environmental Engineering, University of Tennessee, Knoxville, TN 37996, USA*

ABSTRACT

The present study utilizes air quality modeling to probe the sources and characteristics of $PM_{2.5}$ (particles less than 2.5 micrometers in aerodynamic diameter) at the northern tip of Taiwan (CAFE station) in the early stage of the Asian haze period. Since CAFE is the first place that is influenced by the Asian haze coming from the north, this study focused on the wind field, $PM_{2.5}$ concentration, and $PM_{2.5}$ composition at CAFE. During the research period (Oct. 16, 2015, to Nov. 15, 2015), four $PM_{2.5}$ episodes occurred at CAFE. This study classified these four episodes into three types, according to their $PM_{2.5}$ sources: the long-range transport (LRT) type, the local pollution (LP) type, and the LRT/LP mix type. For the LRT type, Asian outflows prevailed in a north to northeast wind at the north of Taiwan. The proportion of NO_3^- in the $PM_{2.5}$ resolvable compositions was very small at CAFE due to evaporation during transport, whereas the relative proportion of sea salt increased due to strong winds. For the LP type, an east wind prevailed and formed a cyclone/lee vortex in northwest Taiwan. Although the background $PM_{2.5}$ concentrations were low (4–20 μg m^{-3}), the cyclone transported local anthropogenic emissions northward and elevated the $PM_{2.5}$ levels at CAFE. For the LRT/LP mix type, an east wind also prevailed, but the background $PM_{2.5}$ concentrations were at an intermediate level (20–30 μg m^{-3}) because the Asian outflows had already transported haze to the West Pacific. The combined LRT and LP increased $PM_{2.5}$ at CAFE. In addition, the proportions of NO_3^- (nitrate) for the LP and LRT/LP episodes were obviously higher than those on the days before and after. This suggests a considerable contribution on $PM_{2.5}$ from LP.

Keywords: $PM_{2.5}$; Asian haze; Long-range transport; Local pollution; Modeling.

INTRODUCTION

Asian haze adversely affects human health. In the source regions of Asian haze, the $PM_{2.5}$ concentrations can reach hundreds of μg m^{-3} (Huang *et al.*, 2014). The transport of Asian haze severely affects the air quality of downwind areas. When the winter monsoon prevails in East Asia, the movements of high-pressure systems usually transport haze from the Asian continent to lee regions. Asian outflows usually dominate air quality in the West Pacific from September to May of the following year. The initial period of haze damage in Taiwan lasts from September to November; December to March of the following year is the most severe period, and April to May is both the ending period and the traditional period in which the northeast monsoon transforms into the southwest monsoon (Chuang *et al.*, 2008a; Wang *et al.*, 2016).

Over the last two decades, extensive research has been conducted on air pollutants and outflows from the Asian continent. These studies included research on outflows of China's dust transport to Northeast Asia (Nishikawa *et al.*, 2000; Kim and Park, 2001; Han *et al.*, 2004; Wang *et al.*, 2012) and even North America (McKendry *et al.*, 2001) or to southern areas, such as Taiwan (Chou *et al.*, 2004; Liu *et al.*, 2006; Lee *et al.*, 2006; Chuang *et al.*, 2008b; Hsu *et al.*, 2010). Lin *et al.* (2004, 2005, 2007) claimed that China's dust transport is usually abundant in cold fronts and reaches Taiwan. Lee *et al.* (2006) observed that in the transportation

* Corresponding author.
Tel.: +886-3-4227151 ext. 34664; Fax: +886-3-4226551
E-mail address: mtchuang100@gmail.com

of dust plumes, $PM_{2.5}$ concentrations, similar to coase mode particulates, were elevated. Simply put, abundant fine-mode particulates reach Taiwan as haze following cold fronts or the prevailing northeast monsoon. Lin *et al.* (2012a) argued that the transport path and boundary conditions near the surface on the way determine the PM_{10} and $PM_{2.5}$ compositions. For example, dust dominates PM_{10}, followed by inorganic ions from anthropogenic emissions. In contrast, $PM_{2.5}$ is dominated by inorganic ions, such as sulfate, nitrate, and ammonium. Lin *et al.* (2012b) suggested that the channel effect over the Taiwan Strait between the Central Mountain Range and Wuyi Mountains can accelerate the transport of air pollutants from northern and eastern China via the East China Sea and influence air quality in Taiwan.

The application of air quality models is useful on the transboundary transport of air pollutants. Chuang *et al.* (2008b) utilized U.S. EPA's Models-3 modeling system/ CMAQ (Community Multiscale Air Quality) to simulate the evolution of chemical components during the long-range transport (LRT) of $PM_{2.5}$ event in a southward high-pressure system from the Asian Continent to Taiwan on Dec 19 and Dec 20 in 2004. During the transport process, the percentage of semi-volatile organic carbon in $PM_{2.5}$ plume only slightly decreased from 22–24% in Shanghai to 21% near Taiwan. However, the percentage of nitrate in $PM_{2.5}$ decreased from 16–25% to 1%. In contrast, the percentage of sulfate in $PM_{2.5}$ increased from16–19% to 35%. In addition, the percentage of ammonium and elemental carbon in $PM_{2.5}$ remained nearly constant. Koo *et al.* (2008) applied the CMAQ model to estimate the contribution of PM_{10} from China emission to Seoul during the high concentration period in January 2007. The results showed that the PM_{10} transport form China to Korea is significant and its contribution reached up to 80% in the episode period. The assessment is very important in managing the air quality improvement plan in Seoul. Aikawa *et al.* (2010) applied the CMAQ model to reproduce the fundamental features of the longitudinal/latitudinal Gradient in the sulfate (SO_4^{2-}) concentrations measured at multiple sites over the East Asian Pacific Rim region. The proportional contribution of Chinese SO_4^{2-} to the total in Japan throughout the year was above 50–70%, using data for Chinese sulfur dioxide (SO_2) emission from the Regional Emission Inventory in Asia, with a winter maximum of approximately 65–80%. The model analysis strongly suggest that the SO_4^{2-} concentrations in Japan were influenced by the outflow from the Asian continent, and this influence was greatest in the areas closer to the Asian continent. Wang *et al.* (2012) applied the CMAQ to simulate the photochemical cycles in the presence of dust particles. With the online dust emission schemes, the CMAQ reproduced reasonable spatial distribution of dust emissions and captured the dust outbreak events. The model system also reproduced observed chemical concentrations, with significant improvements for suspended PM_{10} and aerosol optical depth. Chen *et al.* (2014) used the CMAQ to simulate the effects of East Asia emissions in $PM_{2.5}$ levels in Taiwan by quantifying the direct (LRT of precursors directly forming $PM_{2.5}$ in local areas) and indirect effects (transported precursors interacting with local precursors in forming $PM_{2.5}$). The simulation results indicated that the contributions to annual $PM_{2.5}$ average of 30 $\mu g\ m^{-3}$ in Taiwan are 60, 27, 9, 3%, respectively, from Taiwan's own contribution, direct LRT, indirect LRT and background.

In recent years, air quality forecasts considered the occurrence of invasive haze in Taiwan, particularly in lee areas, where haze is transported from Asian outbreaks, as an early indicator of a deterioration in air quality. When the air quality monitor network in China detects haze in northern or eastern China, forecasters have usually predicted adverse air pollution from LRT at the onset of Asian outbreaks. The present study claims that this condition is not consistently true. Most previous studies regarding LRT focused on the most severe episodes (Chuang *et al.*, 2008b; Lin *et al.*, 2012b). However, no study discussed the impacts of LRT on the early stages of the haze period; i.e., no study has emphasized the presence of air pollutants in outflows from the Asian continent in the commencement of the winter monsoon. The present study simulated autumn from Oct. 16, 2015, to Nov. 15, 2015, which is the beginning of the winter monsoon, and discussed the contributions of LRT and local pollution (LP) to $PM_{2.5}$. The present study discusses the significance of possessing knowledge of the prevailing wind direction and terrain effects. In this study, LRT refers to pollution sources from the Asian continent, and LP is pollution that originates in Taiwan.

METHODS

Study Area and Monitoring Data

The present study applied $PM_{2.5}$ data from six air quality stations to analyze and validate the simulation results. As shown in Fig. 1, Taiwan is located in the West Pacific between East Asia and Southeast Asia. The area is separated from the Chinese mainland by the approximately 200-km-wide Taiwan Strait. During the winter (i.e., from the middle of autumn and winter to spring), Asian high-pressure systems comprise the main air masses over China and the West Pacific. These high-pressure systems drive the East Asian winter monsoon during this period, and the winter monsoon serves as the northeast wind in East Asia (Loo *et al.*, 2015). Cape Fuguei station (Chou *et al.*, 2017, CAFE in Fig. 1) is located at the northern tip of Taiwan, and it receives LRT from the north. LRT from the north may pass Cape Hedo station in Okinawa, Japan (Shimada *et al.*, 2016, HEDO in Fig. 1). To validate the $PM_{2.5}$ concentrations monitored in CAFE station, the current study used data from nearby Wanli (WL in Fig. 1) and Danshui (DA in Fig. 1) stations operated by the Taiwan Environmental Protection Administration (TEPA). We also analyzed $PM_{2.5}$ data from Yangming and Magong (also maintained by TEPA; YM and MG in Fig. 1, respectively) to determine the air quality in the Datun Mountains (827 m a.s.l; located south of CAFE; see Fig. 1) and in a further lee area, respectively. A measurement campaign was held at the CAFE station from Oct. 25, 2015, to Nov. 3, 2015. The campaign included $PM_{2.5}$ sampling and the relevant analysis. In addition to $PM_{2.5}$ concentrations, the present study analyzed the composition of $PM_{2.5}$ observed at CAFE station. The $PM_{2.5}$ compositions

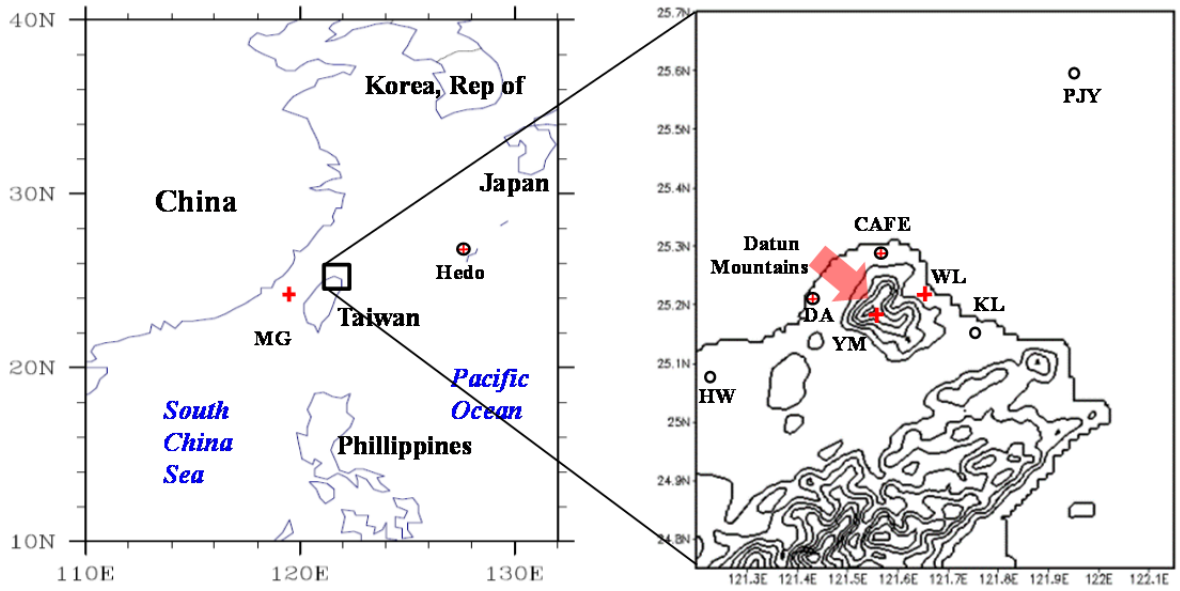

Fig. 1. Geographic location of Taiwan and meteorological (red cross inside black open circle and black open circle: CAFE, DA, KL, HW, and PJY are in the right figure, Hedo is indicated in the left figure) and air quality stations (red cross inside black open circle and red cross: CAFE, DA, WL, MG, YM, and Hedo). CAFE, DA, and Hedo are both meteorological and air quality stations (red cross inside black open circle). Datun mountains is surrounded by DA, CAFE, WL stations. YM is located on Datun mountains.

include water-soluble ions (Na^+, NH_4^+, K^+, Mg^{2+}, Ca^{2+}, Cl^-, NO_3^-, and SO_4^{2-}), organic carbon (OC) and elemental carbon (EC). Sea salt concentration was approximated by $1.47 \times [Na^+] + [Cl^-]$ (in μg m^{-3}), where the factor of 1.47 corresponded to the seawater composition (Quinn and Bates, 2005). For details on the sampling setting and analysis methods, refer to Chou *et al.* (2017).

The present study also used meteorological data (i.e., wind speed, wind direction, and temperature) to evaluate the simulation performance. HEDO station (Shimada *et al.*, 2016) can occasionally determine the meteorological field for Asian outflows when a high-pressure system moves to the West Pacific. Peng Jiayu (PJY in Fig. 1) station is located approximately 60 km northeast of CAFE. This station can present wind fields for the incoming winter monsoon because it is almost unaffected by the terrain of Taiwan Island. MG station can reflect the meteorology in the Taiwan Strait. Keelung (KL in Fig. 1), DA, and Hsinwu (HW) stations are near CAFE and are maintained by the Taiwan Central Weather Bureau. Along with the wind fields of KL, DA, HW, and CAFE stations, we validated the simulated winds around the northern tip of Taiwan.

Model Description and Model Setup

The simulation period for the present study lasted from Oct. 16, 2015, to Nov. 15, 2015. The present study utilized the Weather Research and Forecasting (WRF) Advanced Research WRF Model (version 3.8.1; Skamarock *et al.*, 2008) to generate meteorological data as input for the chemical model. The design of the simulation range features four nested domains. Horizontal resolutions for each domain measured 81, 27, 9, and 3 km, and the corresponding horizontal grids reached 102 × 96, 169 × 166, 223 × 223, and 223 × 223, respectively. Domain 1 is the largest domain and includes East China and Southeast China, whereas Domain 4 is the smallest domain and includes Taiwan alone (Fig. 2). The number of vertical layers totaled 41. Thirteen layers measured below 3,000 m; eight layers were below 1,000 m, with measurements reaching 0, 60, 140, 250, 380, 550, 770, and 1,000 m (these values were not fixed because they varied with air temperature, ground surface height, and surface pressure). These conditions indicate good vertical resolution of the daytime/nighttime boundary layer. The initial conditions for all domains and boundary conditions for Domain 1 were obtained from diagnostic data of the NCEP (National Center for Environmental Prediction, http://www.ncep.noaa.gov/). For the computational mechanism, cumulus parameterization applied the New Grell scheme (Grell *et al.*, 1993); microphysics parameterization applied the scheme by Lin *et al.* (1983); boundary layer parameterization applied YSU (Yonsei University scheme, Hong *et al.* 2006); and longwave and shortwave applied the RRTM (radiation applied rapid radiative transfer model, Mlawer *et al.*, 1997) and Goddard (Chou and Suarez, 1994) scheme. To drive simulated meteorological fields close to actual fields, a simulation applied four-dimensional data assimilation (FDDA); Domains 1 and 2 applied a grid nudge every 6 h of the simulation, and Domains 3 and 4 applied an observation nudge every 3 h of the simulation.

The present study utilized the CMAQ chemical model (version 5.1, Byun and Schere, 2006). To ensure consistency with the meteorological grid structure, CMAQ used the same vertical resolution as WRF. With regard to anthropogenic emissions, Domains 1 to 3 read MICS_Asia (Model Inter-Comparison Study for Asia) 2010 emissions (Li *et al.*, 2017). For Domain 4, emissions were from TEDS 8.1 (Taiwan

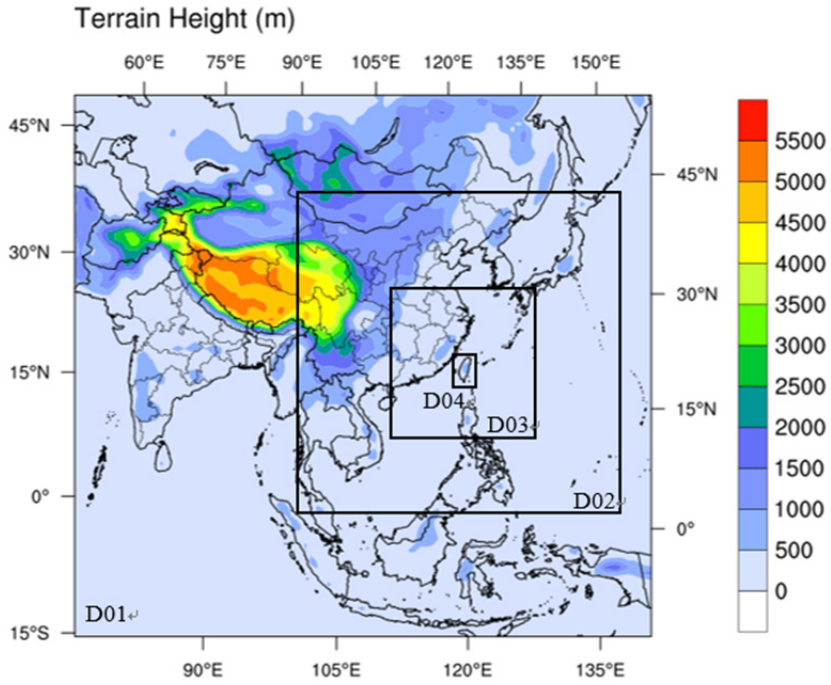

Fig. 2. Configuration of four-level nesting domains in this study.

Emission Database System, TWEPA, 2011) based on the 2010 emission inventory. Afterward, we used the SMOKE (The Sparse Matrix Operator Kernel Emissions, Houyoux and Vukovich, 1999) modeling system to distribute yearly mean TEDS 8.1 emissions into hourly data on each grid. MICS_Asia 2010 and TEDS8.1 emission inventories were for 2010, and they differed from the simulated year in this study, i.e., 2015. This difference possibly had limited effects on the simulation results because no considerable variation was determined for the last several years. MICS_Asia 2010 and TEDS8.1 emission inventories are the most recent public databases, and they are inherently uncertain. The current study applied MEGAN (Model of Emissions of Gases and Aerosols from Nature, Guenther et al, 2012) to derive biogenic emissions for Domains 1 to 3 and applied BEIS-3 (Biogenic Emissions Inventory System-3, Pierce *et al.*, 2002; Schwede *et al.*, 2005) for Domain 4. It is noted that the open fire biomass burning emissions were not included in the present study. The absence of open fire biomass burning emissions may cause underestimation of simulated $PM_{2.5}$ in the LRT plume. However, the underestimation should be acceptable because it accounts for a very limited extent, a few percent to 10 % or so (Huang *et al.*, 2014; Huang *et al.*, 2017).

RESULTS AND DISCUSSION

We first evaluated the performances of the meteorological and chemical simulations. Second, we determined three kinds of episodes that occurred at the CAFE station in the beginning of the haze period. Third, we performed sensitivity tests to support the proposed argument. Finally, we presented and discussed the $PM_{2.5}$ compositions at the CAFE station for those three episodes.

Evaluation of Modeling Results

The evaluation of modeling results involved two parts: an evaluation of meteorology and an evaluation of the $PM_{2.5}$ concentrations. Table 1 summarizes the performances of simulated air temperature, wind direction, and wind speed. This study lists all formulas of statistical evaluation indexes in Supplement S1. The standard for each statistical index is based on Emery (2001) and TWEPA (2016). The evaluation indexes in Table 1 show that the simulated air temperature performed well. This indicates a precise simulation of the air temperature field or the positions of correctly echoed air masses. For wind speed, the among six stations, the simulated wind speed performed well at KL, HW, and PJY stations. However, the simulation overestimated the wind speed at all stations, except at CAFE. The CAFE station is located on the windward side of Datun Mountains (the same location as YM in Fig. 1), with winds coming from the north. The underestimation of simulated wind may be due to the proximity of CAFE to the Datun Mountains. The terrain-blocking effect may be too strong near the CAFE station in the simulation. The DA station is located at the side edge of the Datun Mountains. The flowing simulated air current possibly excessively accelerated around the side edge of the Datun Mountains. The overestimation of wind speed at HEDO station is possibly due to an overestimated northeast wind in the East China Sea. For the wind direction, the simulation performed well at all stations. Moreover, the deviation or error was limited. This implies that the simulation effectively controlled the movement of air currents or micro-to-meso-scale systems around the East China Sea and north of Taiwan.

Table 2 shows the evaluation of $PM_{2.5}$ concentrations at CAFE, DA, WL, YM, MG, and HEDO stations. The standard of evaluation can be found in Emery (2001) and

Table 1. Evaluation of meteorological modeling results for the present study.

		CAFE	DA	KL	HW	PJY	Hedo
Temperature	Observed Avg ± Std (°C)	23.4 ± 1.7	24.0 ± 2.3	23.8 ± 2.0	24.0 ± 1.9	22.9 ± 1.5	24.2 ± 1.5
	Simulated Avg ± Std (°C)	22.6 ± 1.9	23.8 ± 2.2	23.4 ± 1.9	24.0 ± 2.2	23.9 ± 1.0	24.4 ± 1.1
	MB (± 1.5°C)	–0.8	–0.3	–0.4	0.1	1.0	0.2
	MAGE (± 3°C)	1.0	1.1	1.1	0.9	1.3	0.8
	IOA (> 0.6)	1.00	0.94	0.86	0.91	0.71	0.83
Wind speed	Observed Avg ± Std ($m\ s^{-1}$)	7.6 ± 5.0	1.9 ± 1.1	3.0 ± 1.7	6.5 ± 3.6	7.7 ± 2.2	3.6 ± 1.8
	Simulated Avg ± Std ($m\ s^{-1}$)	5.1 ± 2.2	4.2 ± 2.4	4.5 ± 1.6	7.3 ± 3.1	8.3 ± 2.4	7.0 ± 2.7
	MB (± 1.5 $m\ s^{-1}$)	–2.5	2.3	1.5	0.7	0.6	3.4
	RMSE (± 3 $m\ s^{-1}$)	5.1	3.2	2.1	2.1	2.2	4.2
	IOA (> 0.6)	0.63	0.42	0.65	0.90	0.76	0.48
Wind direction	WNMB (± 10%)	–3.8%	–2.0%	2.3%	1.8%	–2.3%	–1.6%
	WNME (± 30%)	10.2%	13.8%	8.7%	7.3%	5.7%	6.8%

Table 2. Evaluation of simulated $PM_{2.5}$ concentration for the present study.

	CAFE	DA	WL	MG	YM	Hedo
OBS Avg ± stdev	21.0 ± 12.1	17.0 ± 12.6	17.7 ± 11.8	22.9 ± 7.4	8.8 ± 10.3	12.6 ± 7.1
SIM Avg ± stdev	14.8 ± 12.7	12.8 ± 11.7	12.8 ± 11.2	9.6 ± 7.1	10.0 ± 9.8	10.5 ± 8.4
MB	–6.2	–1.9	–4.5	–13.1	1.3	–2.1
MAGE	11.0	8.5	9.6	13.4	6.3	8.5
RMSE	14.6	12.4	13.2	15.0	9.2	10.5
MFB (± 60%)	–51.9%	–22.1%	–36.8%	–89.8%	23.0%	–32.0%
MFE (75%)	74.3%	56.8%	67.9%	91.0%	76.0%	78.3%
MNB (–50%~+80%)	–11.3%	–0.5%	–3.0%	–58.3%	127.9%	10.8%
MNE (150%)	70.6%	54.9%	67.1%	59.3%	163.5%	85.2%
NMB (± 85%)	–29.5%	–12.6%	–26.1%	–57.5%	15.3%	–16.6%
NME (85%)	29.5%	12.6%	26.1%	57.5%	15.3%	16.6%
IOA (> 0.6)	0.64	0.72	0.64	0.49	0.76	0.47
R (> 0.35)	0.43	0.49	0.45	0.51	0.59	0.13

Unit: $\mu g\ m^{-3}$ for OBS, SIM, MB, MAGE, RMSE.

TWEPA (2016). As expected, the mean bias (MB) values were negative for all stations as wind speeds were overestimated. Underestimation was more extreme for the MG station, whose MB measured $-13.1\ \mu g\ m^{-3}$. The overestimated southward wind kept the pollutants of Fujian Province, China from moving eastward and forced them to head southward. For other stations, MBs were below the averages or standard deviations of the observed or simulated values. Therefore, the simulation was reasonably executed. For the mean average gross error (MAGE) and root mean square error (RMSE), the MG station performed the worst among the six stations. The MAGE and RMSE of MG were above the average simulated values. The MAGEs for other stations were below the average values or standard deviations of observed and simulated values. RMSEs for the other stations featured the same magnitude as the average values or standard deviations of observed and simulated values. The mean fractional bias (MFB) of MG was larger than –60%, implying an underestimated $PM_{2.5}$ concentration at the MG station. The mean fractional errors (MFEs) of MG, YM, and HEDO stations are slightly higher than 75%. The large MFEs for the YM and HEDO stations were due to some extremely low simulated hourly $PM_{2.5}$ concentrations, which led to large hourly MFEs. Formulas for mean normalized bias (MNB) and mean normalized error (MNE) are similar to MFB and MFE. Therefore, similar to MFE, the MNB and MNE for YM were greater than the standards. Such a condition was also due to some low simulated hourly $PM_{2.5}$ concentrations. Calculation formulas for indexes, such as MNB, MNE, MFB, and MFE, were used to obtain average values of sums of individual ratios. Ratios for some hours may be large when the denominator is small. However, the formulas of normalized mean bias (NMB) and normalized mean error (NME) are similar to those of the ratio of sum of biases to sum of observed values. Therefore, the NMB and NME are more reliable than are the aforementioned indexes. Table 2 shows that the NMB and NME for all stations were below ± 85%. This indicates that the simulation performed well (bias is larger for MG than for the other stations). The index of agreement (IOA) values for CAFE, DA, WL, and YM were high, above 0.6, whereas the IOAs were less than 0.6 for MG and HEDO. One possible cause is that the overestimated wind speed of MG and HEDO resulted in an underestimated $PM_{2.5}$ and, subsequently, immediate IOAs. The correlation coefficients, R, were above 0.35 for all stations, except HEDO. We observed that when air pollutants moved with Asian outflows, they occasionally rapidly moved southward along with the winter monsoon. Therefore, the haze plume may not pass the HEDO station occasionally. The underestimation on

Oct. 19, Nov. 12, and Nov. 13 and the overestimation on Nov. 10–11 were due to biases in simulated rainfall.

Characteristics of $PM_{2.5}$ during High-Concentration Episodes and Related Weather Patterns

Figs. 3(a) to 3(f) present comparisons of hourly observed and simulated $PM_{2.5}$ concentrations at CAFE, DA, WL, YM, MG, and HEDO stations. Four episodes transpired on Nov. 2, Nov. 6, Nov. 7–8, and Nov. 13 when the simulated or observed hourly $PM_{2.5}$ concentration was higher than 35 μg m^{-3} once at CAFE. Fig. 3 clearly shows a consistent trend of simulated and observed $PM_{2.5}$ for CAFE, DA, WL, and YM stations, which are all located over land on Taiwan Island. However, the simulated $PM_{2.5}$ did not perform well at MG and HEDO stations. Nonetheless, we can still discuss the sources of $PM_{2.5}$ from the wind field and the $PM_{2.5}$ concentration distribution. It is noted that the peak on Nov. 6 only occurred at CAFE station but not at nearby DA, WL, and KL stations. Moreover, it is found that the sum of resolvable $PM_{2.5}$ components on Nov. 6 is far less than those on Nov. 7 and Nov. 8 at CAFÉ station (unshown). Therefore, it is reasonable to judge the observed high $PM_{2.5}$ on Nov. 6 is probably due to abnormality of observation device or manual errors. For the simulated peak

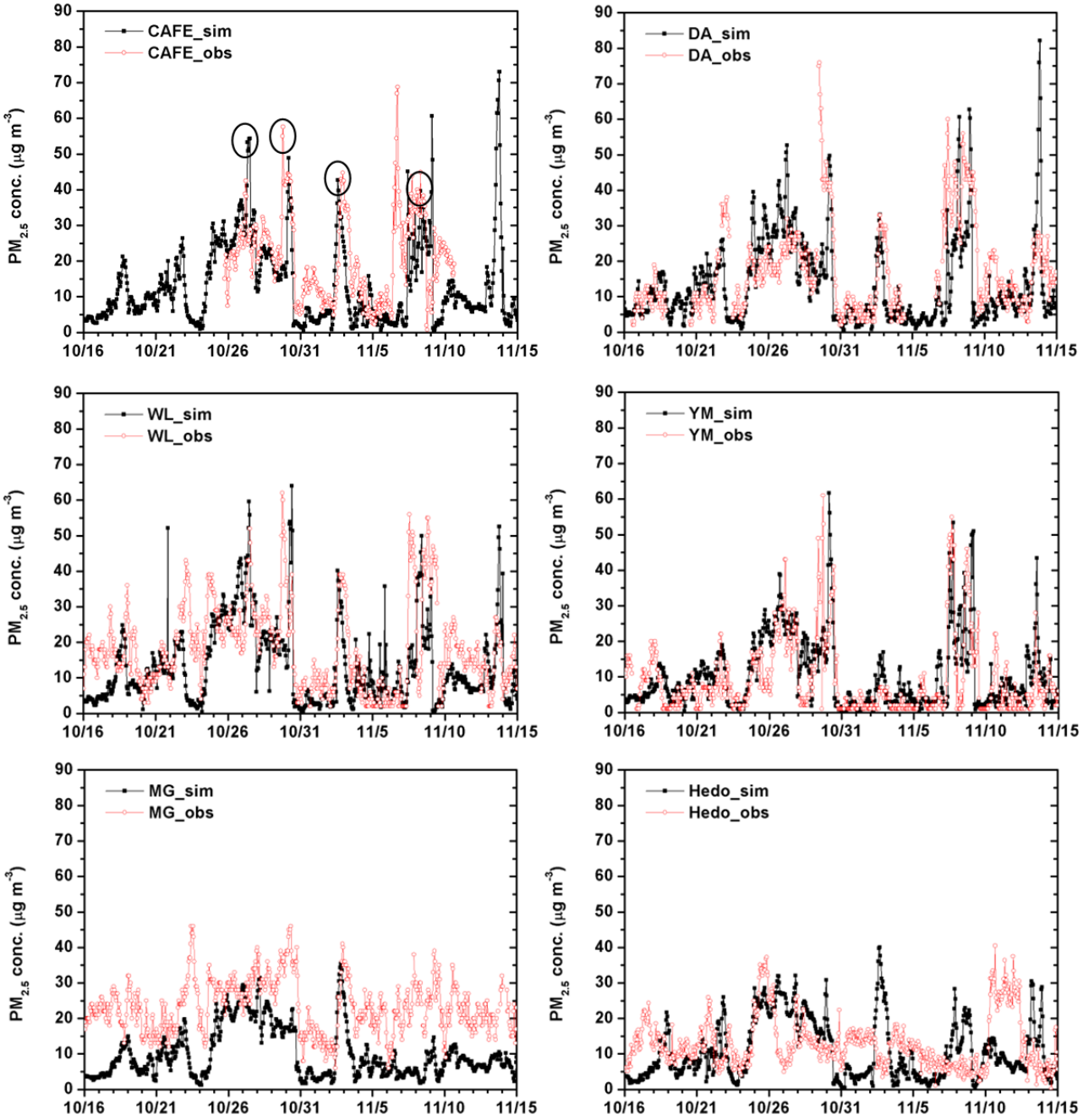

Fig. 3. The time series of hourly simulated (black filled-circle line) and observed (red hollow-circle line) $PM_{2.5}$ at CAFE, YM, WL, YM, MG, and Hedo stations (the four circles indicate four episodes occurring at CAFE during the research period).

on Nov. 13, it is obvious the simulated $PM_{2.5}$ was extremely overestimated. Therefore, it is worthless to discuss the peak on Nov. 13. In conclusion, the present study discussed occurrences on Nov. 2, Oct. 29, and Oct. 26, when sources came from LRT, LP, and LP/LRT mix, respectively. The Nov. 7–8 episode is similar to that of Oct. 29 under the LP type. Thus, this study did not discuss the Nov. 7–8 episode.

LRT Type: Description of Nov. 2 Episode

When the winter monsoon prevails, the northeast wind usually brings air pollutants from the Asian continent to lee areas, such as Taiwan. The path from Shanghai via East China Sea to Taiwan/Taiwan Strait and then to Vietnam formed an air pollutant river (Lin *et al.*, 2012b). Therefore, when the $PM_{2.5}$ concentrations increase at the TWEPA-maintained WL station, air quality forecasts usually consider the initiation of an air quality invasion by an LRT haze plume in northern Taiwan. The Nov 2 episode is such a typical case. Characteristic weather indicated that Asian high-pressure systems rapidly moved southward (Supplement S2(a)).

At 02:00 h on Nov. 2, the simulated $PM_{2.5}$ concentration was below 10 μg m^{-3} around Taiwan, as shown in Fig. 4(a). High $PM_{2.5}$ concentrations in Central and Southern Taiwan were due to local emissions. Figs. 4(b) to 4(d) show that the LRT of haze gradually moved from the north. At 10:00 h on Nov. 2 (Fig. 4(c)), the haze plume has influenced CAFE, and the simulated $PM_{2.5}$ was 21.4 μg m^{-3} (the observed $PM_{2.5}$ reached 19.3 μg m^{-3} at 14:00 h at the CAFE station). At 14:00 h on Nov. 2, the simulated $PM_{2.5}$ peaked at 42.7 μg m^{-3} at the CAFE station (Fig. 4(d)), the observed $PM_{2.5}$ peaked at 42.9 μg m^{-3} at 19:00 h at the CAFE station). Along with the prevailing northeast wind, the haze plume gradually influenced the west side of Taiwan. Because the roughness height on land is higher than that at sea, wind decelerated over western Taiwan. The boundary layer height decreased as the day gradually turned to night (green box #1 in Supplement S3). The simulated $PM_{2.5}$ concentrations rose over the entire west side of Taiwan from 18:00 h on Nov. 2 (Fig. 4(e)) to 22:00 h on Nov. 2 (Fig. 4(f)). Afterward, the haze plume shrank to the west of Taiwan. At 04:00 h on Nov. 3 (Fig. 4(g)), the simulated $PM_{2.5}$ concentration at CAFE dropped to less than 20 μg m^{-3} (the observed $PM_{2.5}$ concentration declined to 18.0 μg m^{-3} at 11:00 h on Nov. 3). At 06:00 h on Nov. 3 (Fig. 4(h)), the simulated $PM_{2.5}$ concentration fell to less than 10 μg m^{-3} (the observed $PM_{2.5}$ concentration declined to 10.3 μg m^{-3} at 14:00 h on Nov. 3).

For this episode, the northeast wind prevailed, which pushed the haze plume from the Asian continent to Taiwan. Therefore, this episode is a classic case of LRT. For details on the variation of $PM_{2.5}$ compositions, refer to Chuang *et al.* (2008a, b). For a discussion of their dynamics, refer to Lin *et al.* (2004, 2005, 2007, 2012a, b).

LP Type: Description of the Oct. 29 Episode

For the Oct. 29 episode, the characteristic weather was the movement of the Asian high-pressure system to the West Pacific. The clockwise peripheral circulation of high-pressure systems flew to the West Pacific and back to Asian continent around Taiwan (Supplement S2(b)). At 16:00 h on Oct. 29, an east wind prevailed east of Taiwan. The dominant east

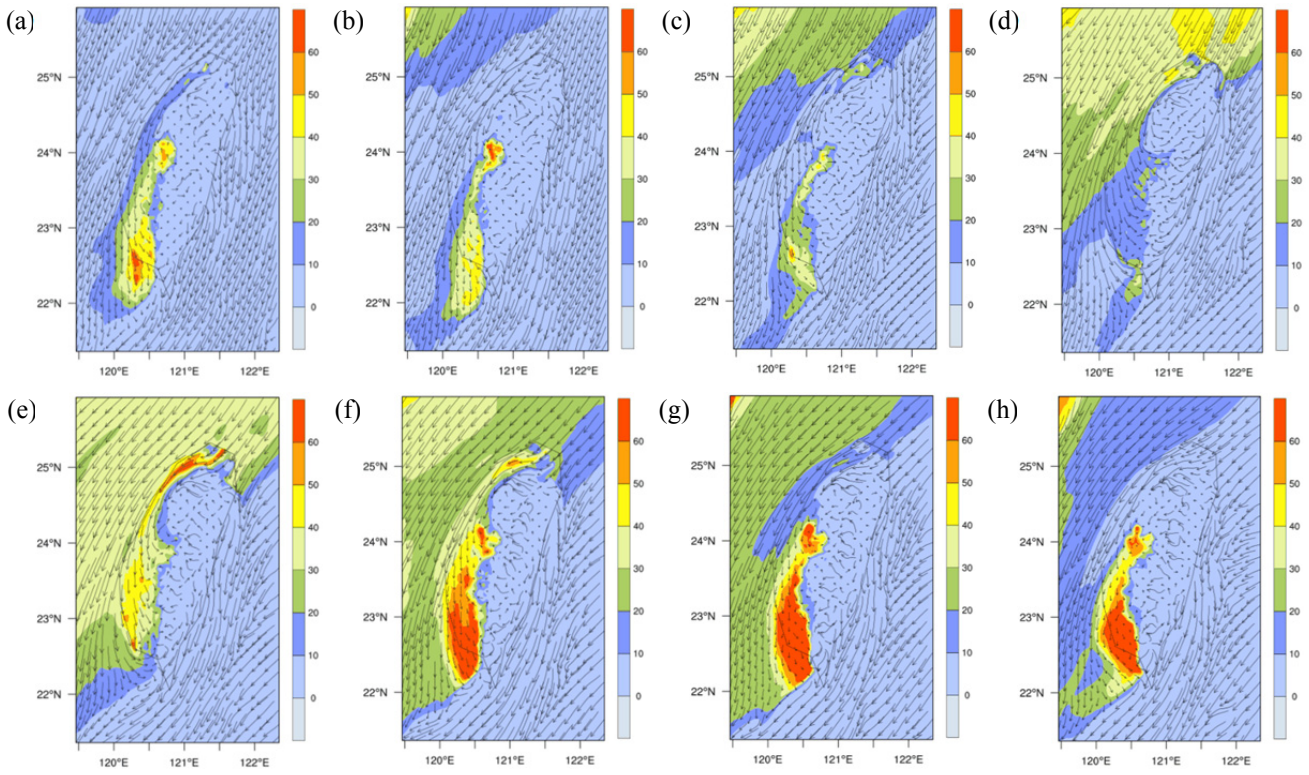

Fig. 4. Simulated wind field and $PM_{2.5}$ concentration distributions at (a) 02:00 Nov. 2; (b) 06:00 Nov. 2; (c) 10:00 Nov. 2; (d) 14:00 Nov. 2; (e) 18:00 Nov. 2; (f) 22:00 Nov. 2; (g) 02:00 Nov. 3; (h) 06:00 Nov. 3.

wind passed by the CAFE station and formed a cyclone over land in northwestern Taiwan (Fig. 5(a)). This cyclone was similar to a lee vortex forming on the lee side of the northern Central Mountains Range (similar to but slightly smaller in size than the lee vortex in Fig. 10(c) of Sun (2016)). In that period, the air quality at the CAFE station was influenced by the air mass from east of Taiwan. The observed $PM_{2.5}$ concentrations at CAFE were between 10 and 20 μg m^{-3} (at 16:00 h, the simulated and observed $PM_{2.5}$ concentrations at the CAFE station measured 16.1 and 21.3 μg m^{-3}, respectively). As the day turned to night, the boundary layer height gradually declined, and the corresponding $PM_{2.5}$ concentration increased (at 16:00 h on Oct. 29, Fig. 5(a) to 20:00 h on Oct. 29, Fig. 5(b), the observed $PM_{2.5}$ concentration at CAFE station reached 32.3 μg m^{-3} at 17:00 h; green box #2 in Supplement S3). The haze plume overlapped with the cyclone. At night, the cyclone/haze plume in northwest Taiwan gradually moved northward to the sea (20:00 h on Oct. 29, Fig. 5(b) to 04:00 h on Oct. 30, Fig. 5(d)). The simulated $PM_{2.5}$ concentration at the CAFE station peaked at 48.9 μg m^{-3} at 04:00 h on Oct. 30. However, the observed $PM_{2.5}$ concentration peaked at 57.6 μg m^{-3} at 19:00 h on Oct. 29. This condition implies that the earlier movement of the actual haze plume was to the north (closer to the CAFE station) or that the range of the haze plume was larger than the simulated haze plume. A southeast wind prevailed in northwest Taiwan, and it pushed the cyclone/haze plume (i.e., local emissions) northward (at 08:00 h on Oct. 30, Fig. 5(e)). When the cyclone moved northward, the haze plume also influenced $PM_{2.5}$ concentrations at CAFE (the simulated $PM_{2.5}$ concentration reached 48.9 μg m^{-3} at 04:00 h on Oct. 30; observed $PM_{2.5}$ remained above 40 μg m^{-3} until 08:00 h on Oct. 30). This situation lasted until the morning of the next day. The boundary layer height increased, and the $PM_{2.5}$ concentration decreased gradually (green box #3 in Supplement S3). In the morning of Oct. 30, a newly incoming high-pressure system influenced northern Taiwan (Fig. 5(f)), subsequently central Taiwan (Fig. 5(g)), and then southern Taiwan (Fig. 5(h)). The prevailing north wind diluted the $PM_{2.5}$ concentration and simultaneously pushed the haze plume near the CAFE station southward (the simulated $PM_{2.5}$ concentration at CAFE decreased to 16.6 μg m^{-3} at 11:00 h on Oct. 30; observed $PM_{2.5}$ concentration decreased to 15.8 μg m^{-3} at 14:00 h on Oct. 30).

The Nov 7–8 episodes (Supplement S2[c]) were similar to the Oct. 29 episode, in which local emissions were the primary sources. The wind fields and $PM_{2.5}$ concentration contours are presented in Supplement S4. In the Nov. 7–8 episodes, the observed background $PM_{2.5}$ concentration was once as low as approximately 4 μg m^{-3}. The Oct. 26 episode was similar to that on Oct. 29. However, the background $PM_{2.5}$ concentration around Taiwan was higher on Oct. 26 than on Oct. 29. Because the background $PM_{2.5}$ concentration around Taiwan can be traced back to the Asian continent, the Oct. 26 episode was defined as a mix-type in this study.

LRT/LP Mix Type: Description of the Oct 26 Episode

The characteristic weather for the Oct. 26 episode (Supplement S2(d)) was similar to that on Oct. 29. At

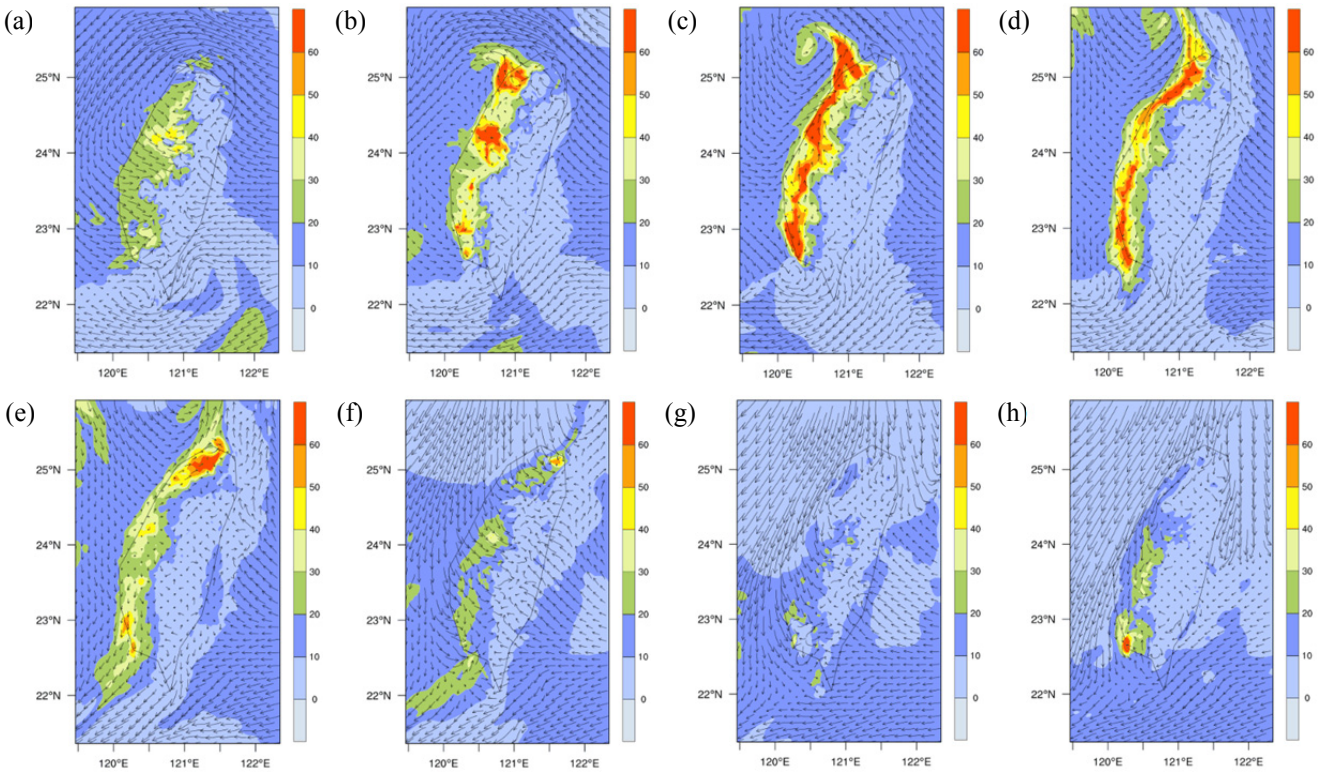

Fig. 5. Simulated wind field and $PM_{2.5}$ concentration distributions at (a) 16:00 Oct. 29; (b) 20:00 Oct. 29; (c) 00:00 Oct. 30; (d) 04:00 Oct. 30; (e) 08:00 Oct. 30; (f) 12:00 Oct. 30; (g) 16:00 Oct. 30; (h) 20:00 Oct. 30.

12:00 h on Oct. 26, the simulated $PM_{2.5}$ concentration at the CAFE station was influenced by LRT from the east. At that point, the simulated $PM_{2.5}$ concentration reached 27.4 μg m^{-3} (the observed $PM_{2.5}$ concentration reached 17.6 μg m^{-3}). Soon, the simulated $PM_{2.5}$ concentration increased to 30 μg m^{-3} at 16:00 h Oct. 26 (Fig. 6(b), the observed $PM_{2.5}$ concentration was 29.4 μg m^{-3} at 21:00 h). A narrow cyclone formed on the west side of Taiwan from the central area to the north, as indicated by yellow to red regions in Fig. 6(c). After 20:00 h (Fig. 6(c)), the prevailing east wind gradually turned to a southeast wind. Narrow cyclones also continually became more evident (Fig. 6(d)). Simultaneously, the simulated boundary layer height decreased, and the simulated $PM_{2.5}$ concentration increased correspondingly (green box #4 in Supplement S3). At 04:00 h on Oct. 27 (Fig. 6(e)), the range of narrow cyclone was restrained in an almost round area. The simulated $PM_{2.5}$ concentration in northwestern Taiwan gradually moved northward (at 08:00 h on Oct. 27, Fig. 6(f)) and transported $PM_{2.5}$ northward. This condition led to an increase in the simulated $PM_{2.5}$ concentration at CAFE station. It is notable that the increase in the $PM_{2.5}$ concentration was due to LP instead of LRT. The near-round-shaped cyclone stayed over northern Taiwan. $PM_{2.5}$ was refined at the northern tip of Taiwan. At 12:00 h on Oct. 27 (Fig. 6(g)), the prevailing wind changed from the south to from the north in northern Taiwan. The prevailing north wind and midday convection over northern Taiwan led to a reduction in $PM_{2.5}$ concentrations. At 16:00 h on Oct. 27 (Fig. 6(h)), the simulated $PM_{2.5}$ concentration at CAFE station decreased again to roughly the same as the background magnitude at approximately 20–30 μg m^{-3} (at 16:00 h–20:00 h Oct. 27, the simulated and observed $PM_{2.5}$ concentrations at CAFE were 26.8–34.2 μg m^{-3} and 15.6–29.6 μg m^{-3}, respectively).

In this episode, the background/LRT haze $PM_{2.5}$ concentration ranged from 20–30 μg m^{-3}. When an east wind prevailed, a cyclone formed in western Taiwan from the central area to the north. Circulation in the cyclone transported local air pollutants to the north and increased the $PM_{2.5}$ concentration at the northern tip of Taiwan. The next section shows that this episode was developed by LRT, which was superimposed on LP. In other words, the difference between the measured $PM_{2.5}$ concentration and 15–30 μg m^{-3} can be considered the contribution from LP.

Sensitivity Test

In previous sections, this study called simulation results the "*base*" case for subsequent discussion. We performed another simulation that removed the anthropogenic emissions of Taiwan. This study calls this simulation the "*none*" case. Fig. 7 displays the comparison of simulated $PM_{2.5}$ concentrations for *base* and *none* cases at the CAFE station. Two small peaks occurred, on Oct. 18 and Oct. 22. The simulated $PM_{2.5}$ concentration for the *base* case almost overlapped with that of *none* case. This phenomenon occurred again during the Nov. 2 episode. This condition suggests that $PM_{2.5}$ at CAFE station was mainly from LRT on Oct. 18, Oct. 22, and Nov. 2. For the Oct. 26, Oct. 29, and Nov. 7–8 episodes, LRT only contributed partly to $PM_{2.5}$ at the CAFE station. The differences resulted from different

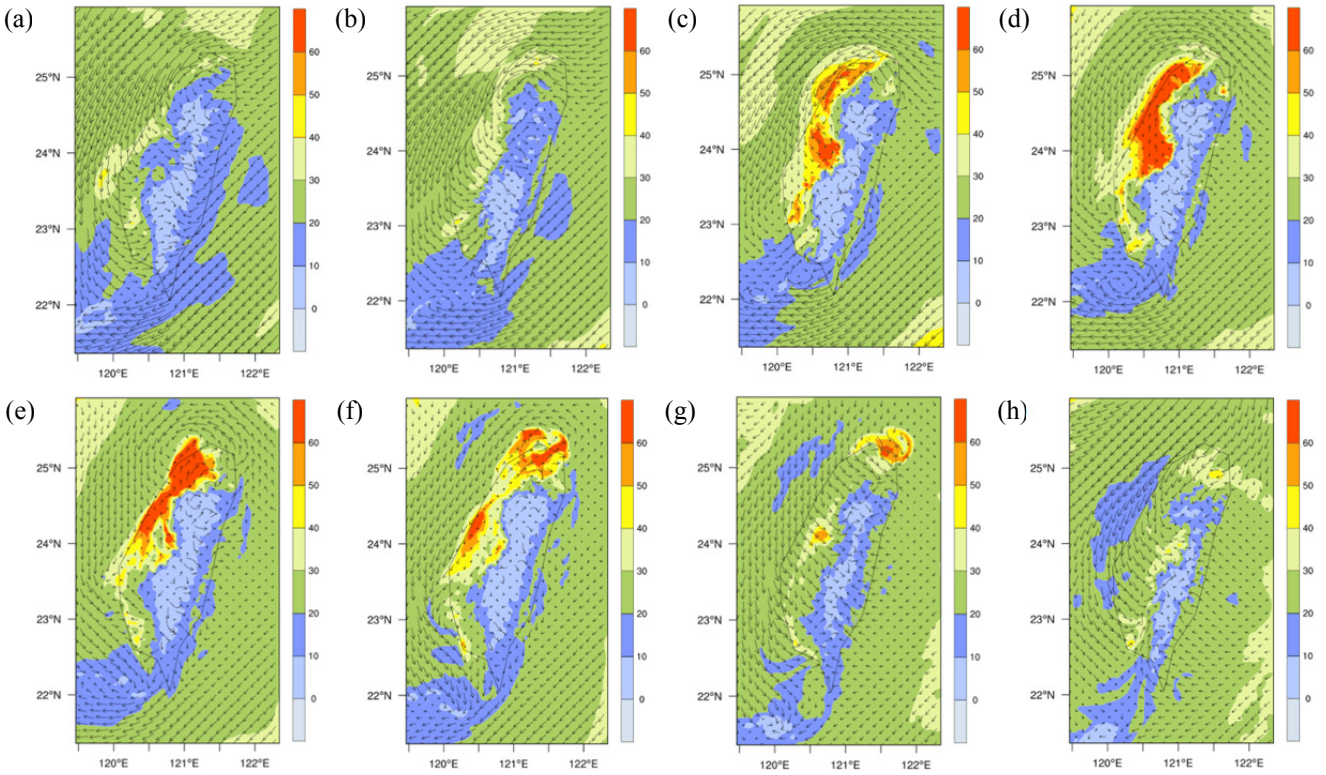

Fig. 6. Simulated wind field and $PM_{2.5}$ concentration distributions at (a) 12:00 Oct. 26; (b) 16:00 Oct. 26; (c) 20:00 Oct. 26; (d) 00:00 Oct. 27; (e) 04:00 Oct. 27; (f) 08:00 Oct. 27; (g) 12:00 Oct. 27; (h) 16:00 Oct. 27.

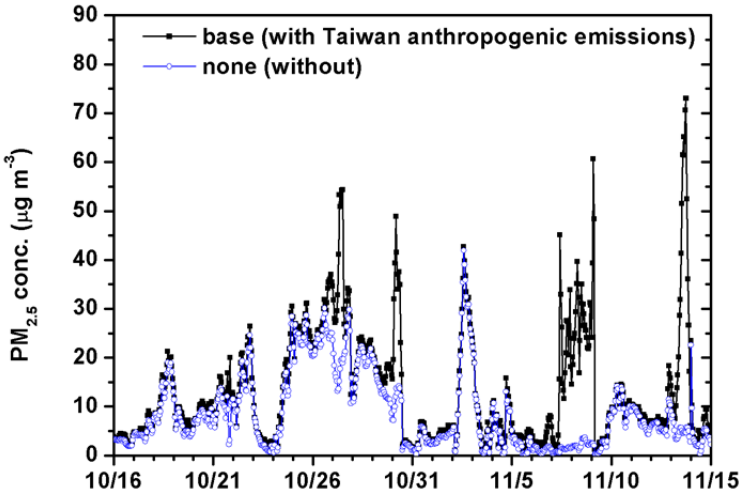

Fig. 7. The $PM_{2.5}$ concentrations for base and none (without Taiwan anthropogenic emissions) cases at Cape Fuguei (CAFE) station.

proportions of LP and LRT. For the Oct. 26 episode, LRT contributed approximately one-third to one-half of $PM_{2.5}$, reaching 20–30 μg m^{-3}. The simulated $PM_{2.5}$ concentrations for the *base* reached 54.3 μg m^{-3} (observed peak was 42.5 μg m^{-3}) because of the contribution from LP. For the Oct. 29 episode, LRT contributed 15–20 μg m^{-3} to simulated $PM_{2.5}$ concentrations. The main contribution was from LP, which increased simulated $PM_{2.5}$ concentrations to nearly 50 μg m^{-3} (the observed peak was 57.6 μg m^{-3}). However, for the Nov. 7–8 episode, the contribution from LRT was lower than those of previous episodes as low as 4 μg m^{-3}, but the total $PM_{2.5}$ concentration measured 20–45 μg m^{-3}. Using sensitivity tests, we gained further insights into the contributions of LP in the present study.

$PM_{2.5}$ Composition Varied before, during, and after Episodes

In this section, this study analyzed the $PM_{2.5}$ composition to gain insights into $PM_{2.5}$ characteristics at CAFE station, whether from the influence of LRT or LP. First, we focused on the Nov. 2, LRT episode. For Nov. 2 (Fig. 8(b)), the proportion of NO_3^- resolvable compositions (the proportions for each component mentioned hereafter are all in $PM_{2.5}$ resolvable compositions; resolvable compositions include inorganics (sulfate, nitrate, ammonium), carbon (organic carbon, element carbon), sea salt (sodium and chlorine), and others (such as magnesium and calcium)) was lower than the day before (Nov 1, Fig. 8(a)) and after (Nov 3, Fig. 8(c)) for the measured *sampler*. This resulted from evaporation of NO_3^- in the haze plume during transport from high to low latitude areas with increasing ambient temperature and aerosol-gas equilibrium between nitrate and nitric acid (Stelson and Seinfeld, 1982; Chuang *et al.*, 2008b). In contrast, the proportions of sea salt were higher on Nov. 1 (Figs. 8(a) and Fig. 8(d)) and Nov. 3 (Figs. 8(c) and Fig. 8(f)) than Nov. 2 (Figs. 8(b) and Fig. 8(e)). Such conditions are due to high wind speed (de Leeuw*et al.*, 2011; Chou *et al.*, 2017). It is obvious that there is difference between samplers and simulations in $PM_{2.5}$ compositions (Fig. 8). The causes included uncertainties such as in the meteorological modeling, emission inventory, chemical mechanisms, and various numerical errors. For example, the ignorance of open file biomass burning in Asian continent could be one of the reasons that caused the deviation in simulated $PM_{2.5}$ compositions.

Next, we discuss the characteristics of sampled $PM_{2.5}$ composition for the LP type episodes on Oct. 29. The proportions of NO_3^- on Oct. 29 (Fig. 9(b)) were higher than on the days before (Oct. 28, Fig. 9(a)) and after (Oct. 30, Fig. 9(c)), even when the quantity of $PM_{2.5}$ was small (most NO_3^- exist in coast mode; Chou *et al.*, 2017). This condition implies that the contribution of LP was higher on Oct. 29. The proportions of EC were the highest on Oct. 29 among all samples. This is probably also related to contributions from the LP. However, the proportions of sea salt were lower on Oct. 29 than on the days before and after. Such a condition is due to low wind speed. In contrast to the Nov. 2 episode (LRT type), the differences in sampled and simulated $PM_{2.5}$ compositions are less on Oct. 29 (LP type) and Oct. 30 than that on Oct. 28. It implies the deviation of simulation may come from the simulated LRT.

Although the proportions of simulated $PM_{2.5}$ components are biased from those of measured samples, the findings showed that the simulation clearly highlighted the aforementioned characteristics. Fig. 9(e) shows that proportions of NO_3^- were highest on Oct. 29 (e.g., Fig. 9(d) for Oct. 28 and Fig. 9(f) for Oct. 30). The result demonstrates that LP contributed considerably to $PM_{2.5}$ concentrations, especially on Oct. 29. The simulated high proportions of NO_3^- for Oct. 29 were not necessarily overestimated compared with the values for synchronous sample, because NH_4NO_3 in $PM_{2.5}$ possibly evaporated from the fine-mode and condensed in a coarse-mode state, e.g., sea salt or dust particles. Simply put, the overestimated proportions of NO_3^- are probably due to the underestimation of sea salt. Next, the proportion of EC was the highest on Oct. 29 but was comparable to that on Nov. 2 (Fig. 8(e)) in the simulation. The simulated EC concentration on Nov. 2 was approximately

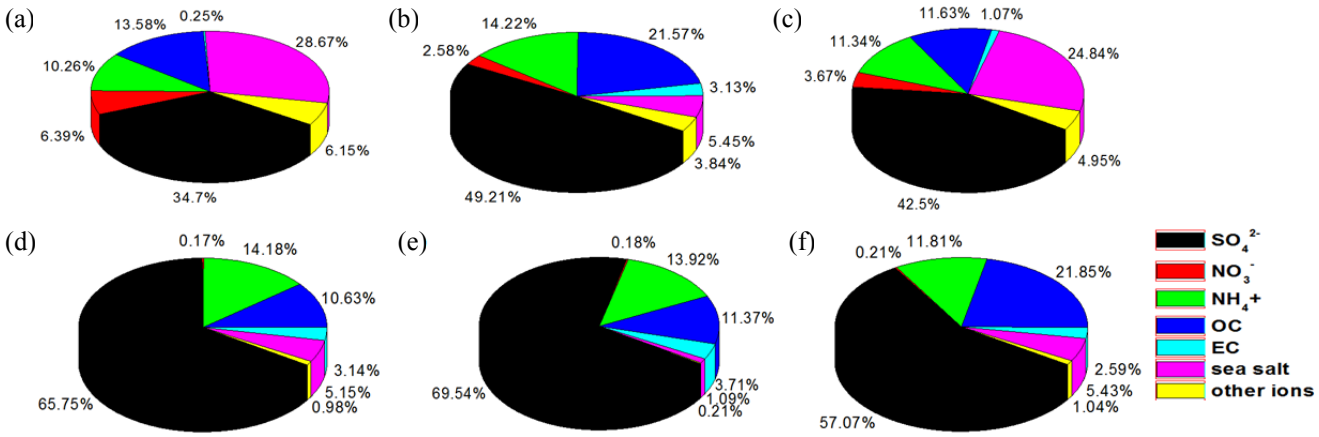

Fig. 8. Pie chart of $PM_{2.5}$ compositions at Cape Fuguei from 08:00 h to 08:00 h (a) sampler, Nov. 1; (b) sampler, Nov. 2; (c) sampler, Nov. 3; (d) simulation with Taiwan anthropogenic emissions, base, Nov. 1; (e) base, Nov. 2; (f) base, Nov. 3.

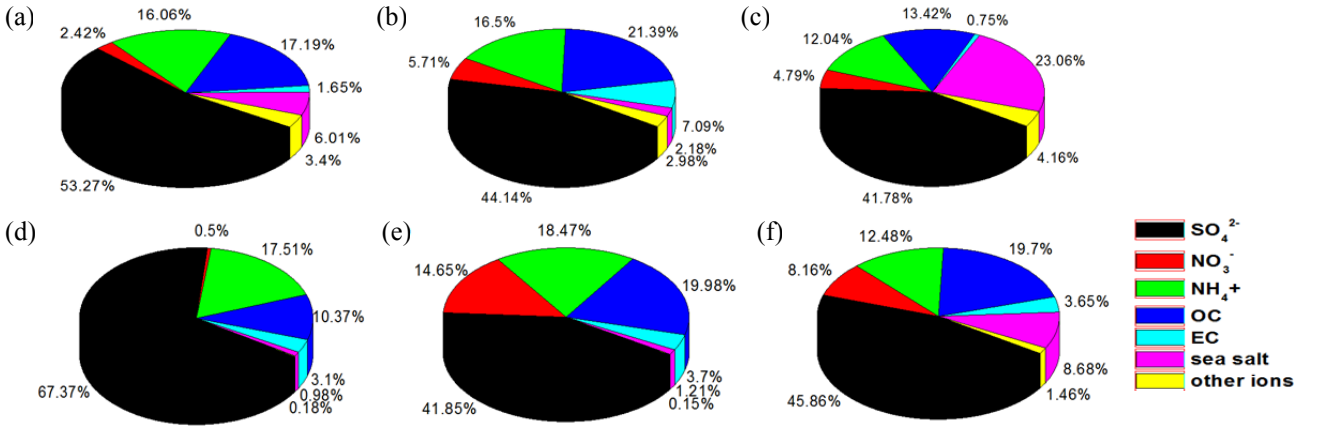

Fig. 9. Pie chart of $PM_{2.5}$ compositions at Cape Fuguei from 08:00 h to 08:00 h (a) sampler, Oct. 28; (b) sampler, Oct. 29; (c) sampler, Oct. 30; (d) simulation with Taiwan anthropogenic emissions, base, Oct. 28; (e) base, Oct. 29; (f) base, Oct. 30.

six times higher than on the days before (Nov. 1, Fig. 8(d)) and after (Nov. 3, Fig. 8(f)). This implies that EC is also high in the haze plume and not a good index for indicating sources from LP.

CONCLUSIONS

The Asian haze following Asian outflows usually influences the $PM_{2.5}$ concentrations in Taiwan. LRT occasionally dominates air quality in northern Taiwan. Most previous studies focused on LRT episodes, especially during the intense stage from December to February of the following year. The present research studied the sources and characteristics of $PM_{2.5}$ at the northern tip of Taiwan (i.e., the CAFE station) in the early Asian haze period, specifically from Oct. 16 to Nov. 15, 2015. This study also performed sensitivity tests to verify the sources of $PM_{2.5}$ at CAFE. Then, we used $PM_{2.5}$ compositions to strengthen our arguments.

Four episodes occurred during the simulation period. This study classified these episodes into three types: the LRT type, the LP type, and the LRT/LP mix type. In the LRT type, Asian outflows prevailed from the north to northeast wind in Taiwan. The haze plume was concentrated at the front of Asian high-pressure systems. Once the haze plume reached CAFE, $PM_{2.5}$ concentrations immediately increased in that area. The proportion of NO_3^- in $PM_{2.5}$ resolvable compositions in the haze plume decreased due to evaporation. The proportion of sea salt increased due to strong winds. For the LP type, when Asian high pressure systems moved to the West Pacific, clockwise peripheral circulation caused a prevailing east wind east of Taiwan. The prevailing east wind brought cleaner air, such that the background $PM_{2.5}$ measured less than 20 μg m^{-3} (possibly less than 10 μg m^{-3}), and formed a cyclone/lee vortex in northwestern Taiwan. The circulation of cyclones brought anthropogenic pollutants (local emissions) over northwestern Taiwan northward to CAFE. The proportion of NO_3^- and EC increased at the CAFE station. For the LRT/LP mix type, when Asian outflows brought Asian haze to the West Pacific, the background concentration increased to 20–30 μg m^{-3} around Taiwan. The prevailing wind for this type was also an east wind. Similarly, a narrow cyclone/lee vortex transported air pollutants northward, and background $PM_{2.5}$ increased $PM_{2.5}$ concentrations at CAFE. The proportions of NO_3^- and EC also increased.

This study provides insights into $PM_{2.5}$ characteristics at the northern tip of Taiwan in the early stage of the Asian haze period. This study will guide air quality forecasters in judging whether they should announce early warnings on invasive Asian haze for Taiwan.

ACKNOWLEDGEMENTS

We express our deep gratitude for the support from the Ministry of Science and Technology (MOST 105-2119-M-008-018-). We would also like to thank the Taiwan Environmental Protection Administration, Research Center for Environmental Change, Academic Sinica, and Japan National Institute of Environmental Science for providing monitoring data to this study. The researchers also acknowledge the contributions of the U.S. National Center for Environmental Prediction, Data Bank of Atmospheric & Hydrologic Research (managed by the Taiwan Typhoon and Flood Research Institute, National Applied Research Laboratories) for input data for meteorological modeling.

SUPPLEMENTARY MATERIAL

Supplementary data associated with this article can be found in the online version at http://www.aaqr.org.

REFERENCES

Aikawa, M., Ohara, T., Hiraki, T., Oishi, O., Tsuji, A., Yamagami, M., Murano, K. and Mukai, H. (2010). Significant geographic gradients in particulate sulfate over Japan determined from multiple-site measurements and a chemical transport model: Impacts of transboundary pollution from the Asian continent. *Atmos. Environ.* 44: 381–391.

Byun, D. and Schere, K.L. (2006). Review of the governing equations, computational algorithms, and other components of the Models-3 Community Multiscale Air Quality (CMAQ) modeling system. *Appl. Mech. Rev.* 59: 51–77.

Chou, C.C.K., Lin, C.Y., Hsu, S.C., Lung, C.S.C., Chen, T.K., Liu, S.C. and Young, C.Y. (2004). Influence of long-range transported dust particles on local air quality: Case study of the Asian dust episodes in Taipei during the spring of 2002. *Terr. Atmos. Ocean. Sci.* 15: 881–899.

Chou, C.C.K., Hsu, W.C, Chang, S.Y., Chen, W.N., Chen, M.J., Huang, W.R., Huang, S.H., Tsai, C.Y., Chang, S.C., Lee, C.T. and Liu, S.C. (2017). Seasonality of the mass concentration and chemical composition of aerosols around an urbanized basin in East Asia. *J. Geophys. Res. Atmos.* 122: 2026–2042.

Chou, M.D. and Suarez, M.J. (1994). An efficient thermal infrared radiation parameterization for use in general circulation models. *NASA Tech. Memo.* 104606: 85.

Chuang, M.T., Chiang, P.C., Chan, C.C., Wang, C.F., Chang, Y.Y. and Lee, C.T. (2008a). The effects of synoptical weather pattern and complex terrain on the formation of aerosol events in the greater Taipei area. *Sci. Total Environ.* 399: 128–146.

Chuang, M.T., Fu, J.S., Jiang, C.J., Chan, C.C., Ni, P.C. and Lee, C.T. (2008b). Simulation of long-range transport aerosols from Asian Continent to Taiwan by a Southward Asian high-pressure system. *Sci. Total Environ.* 406: 168–179.

de Leeuw, G., Andreas, E.L., Anguelova, M.D., Fairall, C.W., Lewis, E.R., O'Dowd, C., Schulz, M. and Schwartz, S.E. (2011). Production flux of sea spray aerosol. *Rev. Geophys.* 49: RG2001.

Emery, C., Tai, E. and Yarwood, G. (2001). Enhanced meteorological modeling and performance evaluation for two Texas ozone episodes. prepared for the Texas Near Non-Attainment Areas through the Alamo Area Council of Governments", by ENVIRON International Corp, Novato, CA., http://www.tnrcc.state.tx.us/air/aqp/airquality_contracts.html# met01.

Grell, G.A. (1993). Prognostic evaluation of assumptions used by cumulus parameterizations. *Mon. Weather Rev.* 121: 764–787.

Guenther, A.B., Jiang, X., Heald, C.L., Sakulyanontvittaya, T., Duhl, T., Emmons, L.K. and Wang, X. (2012). The model of emissions of gases and aerosols from Nature version 2.1 (MEGAN2.1): An extended and updated framework for modeling biogenic emissions. *Geosci. Model Dev.* 5: 1471–1492.

Han, Y.J., Holsen, T.M., Hopke, P.K., Cheong, J.P., Kim, H. and Yi, S.M. (2004). Identification of source locations for atmospheric dry deposition of heavy metals during yellow-sand events in Seoul, Korea in 1998 using hybrid receptor models. *Atmos. Environ.* 38: 5353–5361.

Hong, S.Y., Noh, Y. and Dudhia, J. (2006). A new vertical diffusion package with an explicit treatment of entrainment processes. *Mon. Weather Rev.* 134: 2318–2341.

Houyoux, M. and Vukovich, J. (1999). Updates to the Sparse Matrix Operator Kernel Emissions (SMOKE) modeling system and integration with Models-3. The Emissions Inventory: Regional Strategies for the Future Conference. Air and Waste Management Association, Raleigh, NC.

Hsu, S.C., Liu, S.C., Arimoto, R., Shiah, F.K., Gong, G.C., Huang, Y.T., Kao, S.J., Chen, J.P., Lin, F.J., Lin, C.Y., Huang, J.C., Tsai, F. and Luung, S.C. (2010). Effects of acidic processing, transport history, and dust and sea salt loadings on the dissolution of iron from Asian dust. *J. Geophy. Res.* 115: D19313.

Huang, R.J., Zhang, Y., Bozzetti, C., Ho, K.F., Cao, J.J., Han, Y., Daellenbach, K.R., Slowik, J.G., Platt, S.M. and Canonaco, F. (2014). High secondary aerosol contribution to particulate pollution during haze events in China. *Nature* 514: 218–222.

Huang, X., Yun, H., Gong, Z., Li, X., He, L., Zhang, Y. and Hu, M. (2014). Source apportionment and secondary organic aerosol estimation of $PM_{2.5}$ in an urban atmosphere in China. *Sci. China Earth Sci.* 57: 1352–1362.

Huang, X., Liu, Z., Liu, J., Hu, B., Wen, T., Tang, G., Zhang, J., Wu, F., Ji, D., Wang, L. and Wang, Y. (2017). Chemical characterization and synergetic source apportionment of $PM_{2.5}$ at multiple sites in the Beijing–Tianjin–Hebei region, China. *Atmos. Chem. Phys.* 17:

12941–12962.

Kim, B.G. and Park, S.U. (2001). Transport and evolution of a winter-time Yellow sand observed in Korea. *Atmos. Environ.* 35: 3191–3201.

Koo, Y.S., Kim, S.T., Yun, H.Y., Han, J.S., Lee, J.Y., Kim, K.H. and Jeon, E.C. (2008). The simulation of aerosol transport over East Asia region. *Atmos. Res.* 90: 264–271.

Lee, C.T., Chuang, M.T., Chan, C.C., Cheng, T.J. and Hung, S.L. (2006). Aerosol characteristics from the Taiwan aerosol supersite in the Asian yellow-dust periods of 2002. *Atmos. Environ.* 40: 3409–3418.

Li, M., Zhang, Q., Kurokawa, J., Woo, J.H., He, K., Lu, Z., Ohara, T., Song, Y., Streets, D. and Carmichael, G. (2017). MIX: A mosaic Asian anthropogenic emission inventory for the MICS-Asia and the HTAP projects. *Atmos. Chem. Phys.* 17: 935–963.

Lin, C.Y., Liu, S.C., Chou, C.C.K., Liu, T.H., Lee, C.T., Yuan, C.S., Shiu, C.J. and Young, C.Y. (2004). Long-range transport of Asian dust and air pollutants to Taiwan. *Terr. Atmos. Ocean. Sci.* 15: 759–784.

Lin, C.Y., Liu, S.C., Chou, C.C.K., Huang, S.J., Liu, C.M., Kuo, C.H. and Young, C.Y. (2005). Long-range transport of aerosols and their impact on the air quality of Taiwan. *Atmos. Environ.* 39: 6066–6067.

Lin, C.Y., Wang, Z., Chen, W.N., Chang, S.Y., Chou, C.C.K., Sugimoto, N. and Zhao, Z. (2007). Long-range transport of Asian dust and air pollutants to Taiwan: Observed evidence and model simulation. *Atmos. Chem. Phys.* 7: 423–434.

Lin, C.Y., Chou, C.C.K, Wang, Z., Lung, S.C., Lee, C.T., Yuan, C.S., Chen, W.N., Chang, S.Y., Hsu, S.C., Chen, W.C and Liu, S.C. (2012a). Impact of different transport mechanisms of Asian dust and anthropogenic pollutants to Taiwan. *Atmos. Environ.* 60: 403–418.

Lin, C.Y., Sheng, Y.F., Chen, W.N., Wang, Z., Kuo, C.H., Chen, W.C. and Yang, T. (2012b). The impact of channel effect on Asian dust transport dynamics: A case in southeastern Asia. *Atmos. Chem. Phys.* 12: 271–285.

Lin, Y.L., Farley, R.D. and Orville, H.D. (1983). Bulk parameterization of the snow field in a cloud model. *J. Climate. Appl. Met.* 22: 1065–1092.

Liu, C.M., Young, C.Y. and Lee, Y.C. (2006). Influence of Asia dust storms on air quality of Taiwan. *Sci. Total Environ.* 368: 884–897.

Loo, Y.Y., Billa, L. and Singh, A. (2015). Effect of climate change on seasonal monsoon in Asia and its impact on the variability rainfall in Southeast Asia. *Geosci. Front.* 6: 817–823.

McKendry, I., Hacker, J., Stull, R., Sakiyama, S., Mignacca, D. and Reid, K. (2001). Long-range transport of Asian dust to the lower Fraser Valley, British Columbia, Canada. *J. Geophys. Res.* 106: 2–4.

Mlawer, E.J., Taubman, S.J., Brown, P.D., Iacono, M.J. and Clough, S.A. (1997). RRTM, a validated correlated-k model for the longwave. *J. Geophys. Res.* 102: 16663–16682.

Nishikawa, M., Hao, Q. and Morita, M. (2000). Preparation and evaluation of certified reference materials for Asian mineral dust. *Global Environ. Res.* 4: 103–113.

Pierce, T., Geron, C., Pouliot, G., Kinnee, E. and Vukovich, J. (2002). Integration of the Biogenic Emissions Inventory System (BEIS3) into the Community Multiscale Air Quality (CMAQ) Modeling System. In Proceedings of the AMS 4th Urban Environment Symposium, Norfolk, Virginia, May 20–23.

Quinn, P.K. and Bates, T.S. (2005). Regional aerosol properties: Comparisons of boundary layer measurements from ACE 1, ACE 2, Aerosols99, INDOEX, ACE Asia, TARFOX, and NEAQS. *J. Geophys. Res.* 110: D14202.

Schwede, D., Pouliot, G. and Pierce, T. (2005). Changes to the Biogenic Emissions Inventory System Version 3 (BEIS3). Proceedings of the 4th CMAS Models-3 Users' Conference, Chapel Hill, NC, 26–28 September 2005.

Shimada, K., Takami, A., Kato, S., Kajii, Y., Hasegawa, S., Fushimi, A., Shimizu, A., Sugimoto, N., Chan, C.K., Kim, Y.P., Lin, N.H. and Hatakeyama, S. (2016). Characteristics of carbonaceous aerosols in large-scale Asian wintertime outflows at Cape Hedo, Okinawa, Japan. *J. Aerosol Sci.* 100: 97–107.

Skamarock, W.C., Klemp, J.B., Dudhia, J.D., Gill, O.D., Barker, M., Duda, M.G., Huang, X.Y., Wang, W. and Powers, J.G. (2008). *A description of the advanced research WRF version 3*. NCAR Tech. Note NCAR/TN-475+STR.

Stelson, A.W. and Seinfeld, J.H. (1982). Relative humidity and temperature dependence of the ammonium nitrate dissociation constant. *Atmos. Environ.* 16: 983–992.

Sun, W.Y. (2016). The vortex moving toward Taiwan and the influence of the central mountain range. *Geosci. Lett.* 3: 21

TWEPA (2011). National Air emission trends inventory system management and review (2). Taiwan EPA report, EPA-100-FA11-03-D047, in Chinese.

TWEPA (2016). New air quality modeling and simulation standards. Announced in January 2016.

Wang, K., Zhang, Y., Nenes, A. and Fountoukis, C. (2012). Implementation of dust emission and chemistry into the Community Multiscale Air Quality modeling system and initial application to an Asian dust storm episode. *Atmos. Chem. Phys.* 12: 10209–10237.

Wang, L., Xu, J., Yang, J., Zhao, X., Wei, W., Cheng, D., Pan, X. and Su, J. (2012). Understanding haze pollution over the southern Hebei area of China using the CMAQ model. *Atmos. Environ.* 56: 69–79.

Wang, S.H., Hung, W.T., Chang, S.C. and Yen, M.C. (2016). Transport characteristics of Chinese haze over Northern Taiwan in winter, 2005-2014. *Atmos. Environ.* 126: 76–86.

Received for review, May 25, 2017
Revised, August 14, 2017
Accepted, September 15, 2017